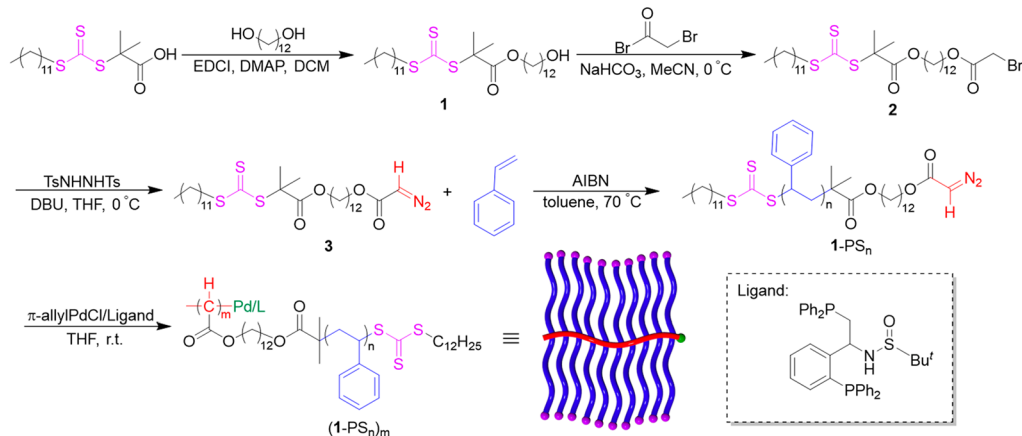


Scheme 1. (A) Synthesis of Bottlebrush Polymer ((1-PS_n)_m) and (B) Synthesis of Amphiphilic Bottlebrush Polymer ((1-PS₃₀)₅₀-b-(2-PEG)₁₀₀)

A: Synthesis of Bottlebrush Polymer with High Graft Density:



B: Synthesis of Amphiphilic Bottlebrush Polymer:

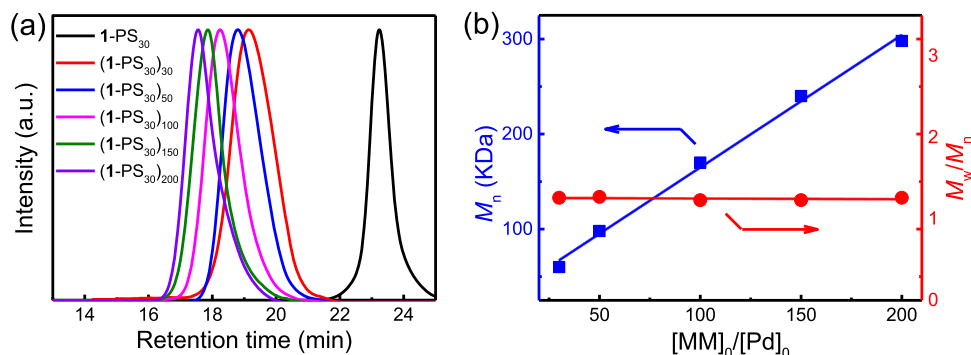
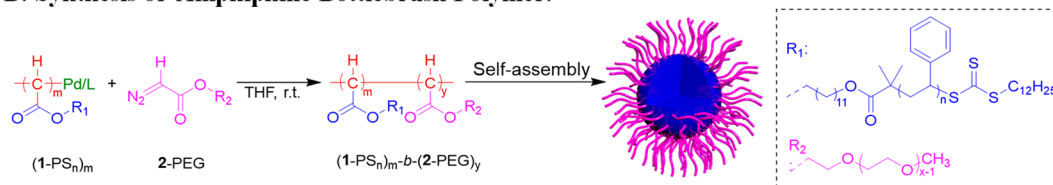


Figure 1. (a) SEC chromatograms of bottlebrush polymers in THF at room temperature with different initial feed ratios. (b) Plot of M_n and M_w/M_n values of bottlebrush polymers as a function of the initial feed ratios of the 1-PS_n macromonomer (MM) to Pd(II). M_n and M_w/M_n were recorded by SEC.

of various diazoacetates and rapidly generate structurally controllable polycarbenes with low polydispersity.^{40,41}

In this work, we report a method to synthesize a series of well-defined bottlebrush polymers via a “grafting-through” strategy, so that each atom of the polycarbene backbone carries a side chain (Scheme 1A). Diazoacetate-terminated macromonomers of 1-PS_n with controlled molecular weight (M_n) and narrow molecular weight distribution (M_w/M_n) were synthesized by the addition–fragmentation chain-transfer (RAFT) polymerization. Interestingly, the diazo can tolerate the RAFT polymerization conditions and remained on the chain end of the yielded PS. The bottlebrush polymers ((1-PS_n)_ms) with controlled M_n s and low M_w/M_n s were prepared by the polymerization of a PS macromonomer using the allyl PdCl/L catalyst at room temperature in an air atmosphere. The polymerization process was carried out in a controllable manner. This demonstrates the unreported functional group tolerance of RAFT polymerization and beautiful compatibility

with the “C1” polymerization employed. It was observed by an atomic force microscope (AFM) that the bottlebrush polymer with a high degree of polymerization (DP) could form a wormlike cylinder shape. Meanwhile, the amphiphilic block polymer brush (1-PS₃₀)₅₀-b-(2-PEG)₁₀₀ was synthesized via the polymerization of diazoacetate macromonomers of PEG (2-PEG) using (1-PS_n)_m with the Pd(II) terminal as the macroinitiator (Scheme 1B). The (1-PS₃₀)₅₀-b-(2-PEG)₁₀₀ could self-assemble into well-defined core–shell micelles. Cytotoxicity tests showed that the core–shell micelles had good biocompatibility.

As shown in Scheme 1A, a new RAFT agent and PS macromonomer (1-PS_n) were prepared according to the reported procedures, and some modifications were made (see Supporting Information for details).^{2,3} The structures were fully characterized by ¹H and ¹³C NMR investigations and Fourier transform infrared (FT-IR) spectra (Figures S1–S5, Supporting Information (SI)). Because of the living nature

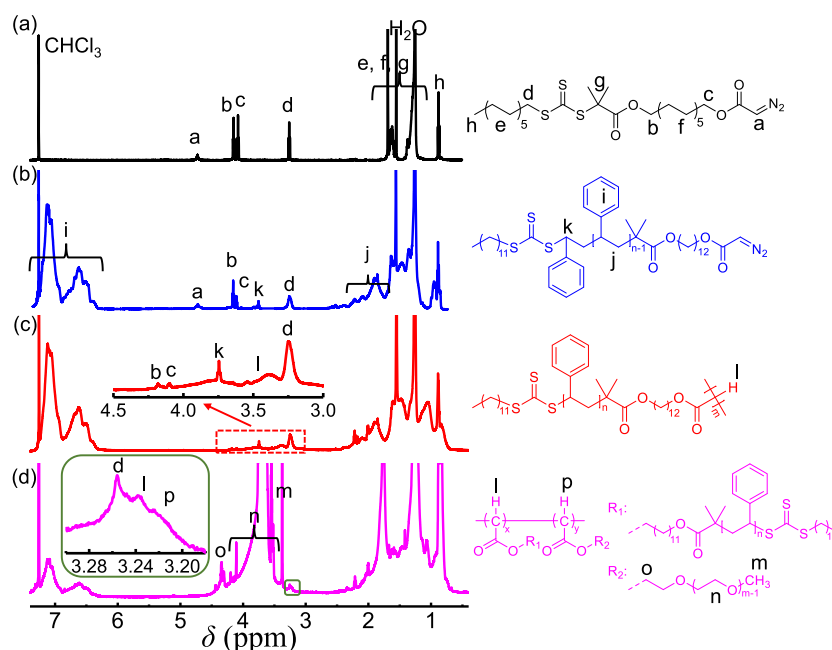


Figure 2. ^1H NMR (600 MHz) spectra of (a) compound 3, (b) 1-PS_{30} macromonomer, (c) $(1\text{-PS}_{30})_{30}$ bottlebrush polymer, and (d) $(1\text{-PS}_{30})_{50}\text{-}(2\text{-PEG})_{100}$ measured in CDCl_3 at 25°C .

of RAFT, the M_n and M_w/M_n of the yielded 1-PS_{30} were, respectively, 2.8 kDa and 1.04, determined by size exclusion chromatography (SEC) (Figure 1a and Table S1 in the SI). The presence of diazo has no negative effect on the RAFT polymerization. The conversion of styrene was up to 84%, and the isolated yield of 1-PS_{30} was 72% because some desired product was lost during the isolation process. The Pd(II)-catalyst-bearing ligand was prepared according to the reported procedures (see SI for details).^{40,41} With 1-PS_n and Pd(II) catalysts in hand, the bottlebrush polymers $(1\text{-PS}_n)_m$ s were synthesized by the polymerizations of 1-PS_n catalyzed by the Pd(II) complexes conducted in THF at room temperature. SEC curves of the separated $(1\text{-PS}_n)_m$ exhibited single modal elution peaks and continually shifted to a higher M_n region with the increased ratio of macromonomer to catalyst (Figure 1a). From the numerical images of the M_n and M_w/M_n values of the generated bottlebrush polymer, it was found that M_n increases linearly, proportional to the ratio of macromonomer to catalyst (Figure 1b). To obtain more details, the polymerization was followed by SEC and ^1H NMR. It revealed that about 70% of 1-PS_{30} was consumed in 15 min. The polymerization followed the first-order reaction mechanism, and the rate constant was 0.11 min^{-1} . The polymerization of the macromonomer was very fast but slower than the small monomers (Figure S6a, SI).^{40,41} Additionally, the M_n of the generated bottlebrushes was linearly correlated to the conversion of 1-PS_{30} , and the dispersity remained narrow with $M_w/M_n < 1.26$ (Figure S6b, SI). The research indicated that the polymerization of the diazoacetate-terminated macromonomer of 1-PS_n by the Pd(II) catalyst proceed in a living manner. Using this method, a variety of bottlebrush polymers were prepared. All the bottlebrush polymers had expected M_n and low dispersity with $M_w/M_n < 1.26$ (Table S2, SI). It was worth mentioning that the isolated yield of the bottlebrush polymers was not very high (42%–59%) probably because the side reaction of diazoacetate dimerization made the isolation of bottlebrushes from the dimer quite difficult, and some product

might be lost during solvent fractionation. Notably, when the DP of 1-PS_n reached 40, it was difficult for the polymerization to take place due to the steric hindrance. Because the side chains of the bottlebrushes were compactly packed together and the ester linkages were wrapped inside, saponification of the esters to title the grafting density failed.

Besides SEC analyses, the polymers were verified by ^1H and ^{13}C NMR and FT-IR spectra. ^1H NMR spectra supported the formation of expected polymers with accepted purity (>95%). Characteristic resonances coming from the phenyl pendants and the backbone were clearly discerned. For instance, from the ^1H NMR spectra of compound 3 (Figure 2a) and 1-PS_{30} (Figure 2b), the signal at 4.73 ppm (peak a), which came from the N_2CH of the diazo group, could be clearly observed. Based on the integral analysis of terminal N_2CH (peak a, 4.73 ppm) and repeating units of the benzene ring (peak i, 7.81–6.45 ppm), the DP of PS was ca. 27, which generally agreed with the SEC analyses.

However, the resonance of N_2CH disappeared in the ^1H NMR spectrum of the $(1\text{-PS}_{30})_{30}$ bottlebrush polymer as shown in Figure 2c, indicating the formation of the main chain. In addition, signals at 7.81–6.45 ppm (peak i) could be safely ascribed to the resonances of phenyl protons, while the resonance at 3.84–3.75 (peak k) and 2.61–1.74 (peak j) came from the CH and CH_2 that connected on the benzene ring. The signal of the main-chain CH proton was located at 3.52–3.31 ppm with a broad peak (peak l). Moreover, FT-IR spectra further confirmed that we had successfully prepared bottlebrush polymers by the PS macromonomer with a diazo group at the chain end (Figure S7, SI).

AFM was used to observe the images of synthetic bottlebrush polymers with different backbone DPs but the same side-chain length. The $(1\text{-PS}_{30})_m$ showed extended wormlike morphology. As illustrated in Figure 3a and Figure S8a in the SI, on account of the low DP of the backbone, $(1\text{-PS}_{30})_{50}$ displayed a spherical shape with a mean diameter of ca. 20 nm. The image of $(1\text{-PS}_{30})_{100}$ changed to an ellipsoid-like

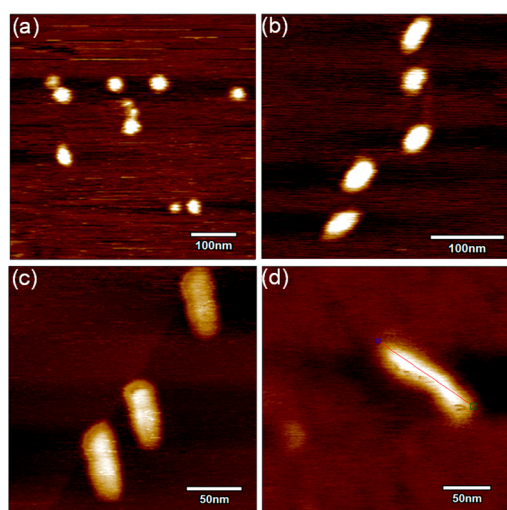


Figure 3. AFM images of bottlebrush polymers with different main-chain lengths: (1-PS₃₀)₅₀ (a), (1-PS₃₀)₁₀₀ (b), (1-PS₃₀)₁₅₀ (c), and (1-PS₃₀)₂₀₀ (d) casted from THF solutions on mica.

shape with the increased backbone DP (Figure 3b and Figure S8b in the SI). Then, the AFM height image of (1-PS₃₀)₁₅₀ exhibited a wormlike morphology on mica lamination with a further increase in the backbone DP (Figure 3c and Figure S8c in the SI), while the mean length of the wormlike cylinders was 50 nm. (1-PS₃₀)₂₀₀ adopted a more obvious wormlike morphology with the increase of DP, and the average length of (1-PS₃₀)₂₀₀ was ca. 75 nm (Figure 3d and Figure S8d in the SI). Since the widths of the grafted side chain were constant with the same chain length, the widths were almost the same, about 20 nm. Moreover, the heights of the wormlike morphologies were around 2.0–2.5 nm (Figure S8, SI). Those low heights might be due to the low DP of the side chain, and the other reason might be the side chains of the bottlebrush polymer laid on the AFM substrate due to their strong interaction with the mica.

After the successful obtainment of the (1-PS₃₀)_m, we then tried to synthesize the amphiphilic bottlebrush polymers, which could be used for drug delivery. First, the diazoacetate macromonomer of 2-PEG was synthesized (see SI for details). The amphiphilic bottlebrush polymer with PS as a hydrophobic segment and PEG as a hydrophilic segment was prepared according to Scheme 1B. SEC, ¹H NMR, and FT-IR analyses of the yielded (1-PS₃₀)₅₀-b-(2-PEG)₁₀₀ indicated that the copolymerization was successful (Figure 2d and Figures S9 and S10 in the SI). It could be seen that the elution trace of the (1-PS₃₀)₅₀-b-(2-PEG)₁₀₀ was changed after the introduction of the hydrophilic segment (Figure 4a). Because PEG and PS exhibit different hydrodynamic volume in THF, just a slight SEC shift was observed. The *M_n* and *M_w/M_n* of the block copolymer brush were 67.0 kDa and 1.22, respectively. The *M_n* was increased compared to that of the (1-PS₃₀)₅₀ precursor (*M_n* = 50.0 kDa). Due to the amphiphilic character of (1-PS₃₀)₅₀-b-(2-PEG)₁₀₀, it had good solubility in many solvents which caused the solvent fractionation to be quite difficult, and the isolation yield was just ca. 50%.

In addition, the ¹H NMR spectrum further supported the formation of the anticipated amphiphilic bottlebrush polymer. The characteristic resonances from the PS side chain and the PEG side chain could be clearly identified (Figure 2d), such as the signals at 7.23–6.34 ppm due to the resonances of phenyl

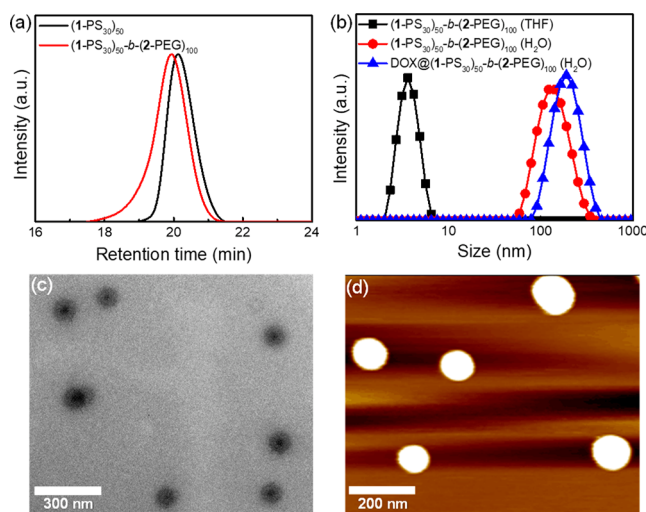


Figure 4. (a) SEC chromatograms of (1-PS₃₀)₅₀-b-(2-PEG)₁₀₀ and (1-PS₃₀)₅₀. (b) DLS of (1-PS₃₀)₅₀-b-(2-PEG)₁₀₀ in THF and (1-PS₃₀)₅₀-b-(2-PEG)₁₀₀ and DOX@(1-PS₃₀)₅₀-b-(2-PEG)₁₀₀ in H₂O. (c) TEM and (d) AFM images of (1-PS₃₀)₅₀-b-(2-PEG)₁₀₀ casted from the aqueous solutions at room temperature.

protons from PS side chains and the signals at 4.37–3.49 ppm ascribed to the resonances of OCH₂ and CH₂ from PEG side chains. The signal of the main-chain CH proton was located at 3.25–3.19 ppm and was split into doublets in the ¹H NMR spectrum of (1-PS₃₀)₅₀-b-(2-PEG)₁₀₀, which was slightly different from that of (1-PS₃₀)₃₀. Furthermore, FT-IR results further confirmed that the (1-PS₃₀)₅₀-b-(2-PEG)₁₀₀ was prepared successfully (Figure S10, SI).

The (1-PS₃₀)₅₀-b-(2-PEG)₁₀₀ was composed of a hydrophobic PS segment and a hydrophilic PEG segment, so we speculated that it could self-assemble into core–shell structure micelles in water. The critical micelle concentration (CMC) is an indispensable index to characterize the structural stability of amphiphilic polymers.⁴² Using the fluorescent probe (pyrene), the CMC of (1-PS₃₀)₅₀-b-(2-PEG)₁₀₀ was determined by the fluorescence investigation, and its value was calculated to be 90 mg/L (Figures S11 and S12, SI).

The hydrodynamic diameter of (1-PS₃₀)₅₀-b-(2-PEG)₁₀₀ was investigated by dynamic light scattering (DLS). The results demonstrated it was dissolved molecularly in THF with a hydrodynamic diameter (*D_h*) of ca. 6 nm (Figure 4b and Table S3 in the SI), while it formed a micelle in water with a *D_h* of ca. 146 nm and polydispersity (PDI) of 0.100. In addition, the morphology of micelles assembled by (1-PS₃₀)₅₀-b-(2-PEG)₁₀₀ was further studied by AFM and transmission electron microscopy (TEM). We observed the formation of spherical micelles by AFM and TEM in Figure 4c and 4d. The mean diameter of the micelle measured by TEM and AFM was estimated to be 140 and 135 nm, respectively, which was almost consistent with the result of DLS analysis. From the TEM image, the core–shell structure micelles could be clearly seen. As is well known, the size of the carrier is usually requested to be less than 200 nm because it plays a significant role in drug delivery through the systemic circulation.⁴³ Therefore, the size of the micelle self assembled by (1-PS₃₀)₅₀-b-(2-PEG)₁₀₀ was suitable for drug delivery applications.

The *D_h* of the prepared core–shell structure micelle was 146 nm (Figure 4b), which might be beneficial to its entry into cancer cells via the enhanced permeability and retention

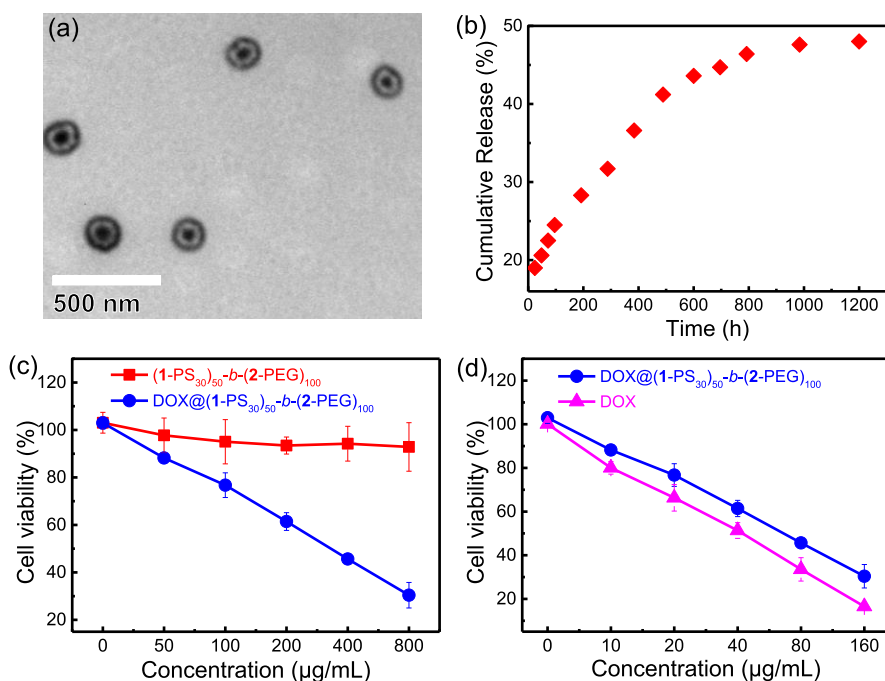


Figure 5. (a) TEM image of $\text{DOX}@(\text{1-PS}_{30})_{50}\text{-}b\text{-(2-PEG)}_{100}$ casted from the aqueous solution at room temperature. (b) DOX release profiles of $\text{DOX}@(\text{1-PS}_{30})_{50}\text{-}b\text{-(2-PEG)}_{100}$ in deionized water. (c) Viability of HeLa cells after incubation with $(\text{1-PS}_{30})_{50}\text{-}b\text{-(2-PEG)}_{100}$ and $\text{DOX}@(\text{1-PS}_{30})_{50}\text{-}b\text{-(2-PEG)}_{100}$ at various polymer concentrations for 48 h. (d) Viability of HeLa cells after incubation with $\text{DOX}@(\text{1-PS}_{30})_{50}\text{-}b\text{-(2-PEG)}_{100}$ and free DOX at various DOX concentrations for 48 h. The error bars are based on the standard deviations of four parallel tests.

(EPR) effect. To explore the micelle in the field of drug release, solvatochromic Nile red (NR) was encapsulated into the $(\text{1-PS}_{30})_{50}\text{-}b\text{-(2-PEG)}_{100}$ micelles to form a $\text{NR}@(\text{1-PS}_{30})_{50}\text{-}b\text{-(2-PEG)}_{100}$ complex micelle using a cosolvent approach (see SI for details). The resulting $\text{NR}@(\text{1-PS}_{30})_{50}\text{-}b\text{-(2-PEG)}_{100}$ displayed a strong fluorescence of NR in deionized water, which confirmed the successful encapsulation of NR into $(\text{1-PS}_{30})_{50}\text{-}b\text{-(2-PEG)}_{100}$ (Figure S13, SI). Without a stimulating response, the fluorescence intensity (I_{630}) of NR gradually thinned, indicating that the NR could be released naturally from the core–shell structure micelle. Then, the quantitative relationship between the released NR and time was studied by fluorescence spectroscopy. After 12 days, the fluorescence intensity of $\text{NR}@(\text{1-PS}_{30})_{50}\text{-}b\text{-(2-PEG)}_{100}$ reached equilibrium, decreasing by a total of 72%. Those results showed that the encapsulated NR was released from the core–shell structure micelle without any stimulation, and core–shell structure micelles had good applications in loading hydrophobic drug molecules.

Finally, the anticancer drug doxorubicin (DOX) was embedded in the $(\text{1-PS}_{30})_{50}\text{-}b\text{-(2-PEG)}_{100}$ micelle to form the $\text{DOX}@(\text{1-PS}_{30})_{50}\text{-}b\text{-(2-PEG)}_{100}$ complex micelle due to its high curative effect. DLS study indicated the D_h increased to 190 nm with PDI = 0.129. The loading capacity of DOX was calculated to be ~25% w/w. As could be seen from Figure 5b, the $\text{DOX}@(\text{1-PS}_{30})_{50}\text{-}b\text{-(2-PEG)}_{100}$ complex micelles had a much larger D_h than the blank micelles. Fluorescence spectroscopy showed that DOX was successfully wrapped in micelles (Figure S14, SI). From the TEM image, a typical spherical morphology of $\text{DOX}@(\text{1-PS}_{30})_{50}\text{-}b\text{-(2-PEG)}_{100}$ was observed (Figure 5a). Compared with the micelle of $(\text{1-PS}_{30})_{50}\text{-}b\text{-(2-PEG)}_{100}$ (Figure 4c), it showed a larger size and more obvious core–shell structure that was due to the encapsulation of DOX molecules in the cores. The release of

DOX from the micellar $\text{DOX}@(\text{1-PS}_{30})_{50}\text{-}b\text{-(2-PEG)}_{100}$ system was further studied by a fluorescence test. The drug release profile could be divided into the two phases, i.e., a shorter release period with a higher release rate within the first 24 h and a slow and continuous release period where almost the entire drug load was delivered from the micelle after 50 days (Figure 5b). The DOX released after incubation for 24 h was 19%, and in total the $\text{DOX}@(\text{1-PS}_{30})_{50}\text{-}b\text{-(2-PEG)}_{100}$ micellar system released ~48% of DOX in deionized water.

To test DOX-encapsulated micelles of $\text{DOX}@(\text{1-PS}_{30})_{50}\text{-}b\text{-(2-PEG)}_{100}$ for the biocompatibility, HeLa cells were incubated with micelles of varying concentrations at 37 °C for 48 h. First, the in vitro dose-dependent cytotoxicity of pure $(\text{1-PS}_{30})_{50}\text{-}b\text{-(2-PEG)}_{100}$, $\text{DOX}@(\text{1-PS}_{30})_{50}\text{-}b\text{-(2-PEG)}_{100}$, and pure DOX was investigated systematically by an MTT assay. It could be clearly seen from Figure 5c and 5d that pure $(\text{1-PS}_{30})_{50}\text{-}b\text{-(2-PEG)}_{100}$ had little cytotoxic effect on cancer cells. Therefore, it could be concluded that micelles had little cytotoxicity and good biocompatibility. However, when HeLa cells were incubated with $\text{DOX}@(\text{1-PS}_{30})_{50}\text{-}b\text{-(2-PEG)}_{100}$ and free DOX at 37 °C, the cell activity decreased remarkably. For the pure DOX, it was obvious that the cell death rate increased linearly with the increase of the DOX concentration (Figure 5d). It could be seen that DOX had great use in killing cancer cells. Compared with the pure DOX, the $\text{DOX}@(\text{1-PS}_{30})_{50}\text{-}b\text{-(2-PEG)}_{100}$ had a slight cytotoxicity at a low micelle concentration (10 µg/mL), but when the concentration increased, the cytotoxicity increased significantly. From Figure 5c and d, about 70% of HeLa cells was destroyed at the concentration of 160 µg/mL of DOX after 48 h incubation. These results showed that the DOX-loaded micelles had a good effect on the chemotherapy of cancer cells.

In summary, we synthesized high densely grafted bottle-brush polymers carrying a polymeric side chain on every

backbone atom catalyzed by the allyl PdCl/L catalysts with rigid bidentate phosphine ligands. We demonstrated the synthesis of (1-PS)_n_m with PS as the side chain in this way and prepared the amphiphilic (1-PS₃₀)₅₀-b-(2-PEG)₁₀₀ using (1-PS₃₀)_m with the Pd(II) terminal as the macroinitiator. The polymerization was carried out in a living manner and provided bottlebrush polymers with tunable composition, quantitative M_n , low M_w/M_n , and high grafting density. The amphiphilic (1-PS₃₀)₅₀-b-(2-PEG)₁₀₀ was able to form core-shell structure micelles for the as-prepared drug. The core-shell structure micelles greatly improved the water solubility of the drug by inhibiting the aggregation of the drug in an aqueous environment. AFM, TEM, and DLS analyses showed that core-shell structure micelles could be used for drug delivery in organisms. Cytotoxicity tests confirmed that the micelles had good biocompatibility. This work provided a synthetic route for accurate synthesis of bottlebrush polymers with high grafting density, and the synthesized bottlebrush polymers could be used in drug delivery. In a later work, we are going to explore the application of bottlebrush polymers in other new functional materials.

■ ASSOCIATED CONTENT

Supporting Information

The Supporting Information is available free of charge at <https://pubs.acs.org/doi/10.1021/acsmacrolett.1c00706>.

Materials and instruments; details of synthesis; and characterization data (PDF)

■ AUTHOR INFORMATION

Corresponding Authors

Na Liu – Department of Polymer Science and Engineering, School of Chemistry and Chemical Engineering, and Anhui Key Laboratory of Advanced Functional Materials and Devices, Hefei University of Technology, Hefei, Anhui Province 230009, China; Email: liuna@hfut.edu.cn

Zong-Quan Wu – Department of Polymer Science and Engineering, School of Chemistry and Chemical Engineering, and Anhui Key Laboratory of Advanced Functional Materials and Devices, Hefei University of Technology, Hefei, Anhui Province 230009, China; State Key Laboratory of Supramolecular Structure and Materials, College of Chemistry, Jilin University, Changchun 130012, China; orcid.org/0000-0001-6657-9316; Email: zqwu@jlu.edu.cn, zqwu@hfut.edu.cn

Authors

Meng-Qing Wang – Department of Polymer Science and Engineering, School of Chemistry and Chemical Engineering, and Anhui Key Laboratory of Advanced Functional Materials and Devices, Hefei University of Technology, Hefei, Anhui Province 230009, China

Hui Zou – Department of Polymer Science and Engineering, School of Chemistry and Chemical Engineering, and Anhui Key Laboratory of Advanced Functional Materials and Devices, Hefei University of Technology, Hefei, Anhui Province 230009, China; orcid.org/0000-0002-6716-9746

Wen-Bin Liu – Department of Polymer Science and Engineering, School of Chemistry and Chemical Engineering, and Anhui Key Laboratory of Advanced Functional Materials

and Devices, Hefei University of Technology, Hefei, Anhui Province 230009, China

Complete contact information is available at: <https://pubs.acs.org/doi/10.1021/acsmacrolett.1c00706>

Author Contributions

§M.-Q.W. and H.Z. contributed equally.

Notes

The authors declare no competing financial interest.

■ ACKNOWLEDGMENTS

This work is supported by the National Natural Science Foundation of China (NSFC, Nos. 21971052, 22071041, 21871073, and 51803045). N. Liu and Z.-Q. Wu thank the Fundamental Research Funds for the Central Universities of China (Grant Nos. PA2019GDPK0057 and PA2020GDJQ0028).

■ REFERENCES

- (1) Feng, C.; Li, Y.; Yang, D.; Hu, J.; Zhang, X.; Huang, X. Well-defined graft copolymers: from controlled synthesis to multipurpose applications. *Chem. Soc. Rev.* **2011**, *40*, 1282–1295.
- (2) Verduzco, R.; Li, X.; Pesek, S. L.; Stein, G. E. Structure, Function, Self-assembly, and Applications of Bottlebrush Copolymers. *Chem. Soc. Rev.* **2015**, *44*, 2405–2420.
- (3) Li, B.; Yu, B.; Ye, Q.; Zhou, F. Tapping the Potential of Polymer Brushes through Synthesis. *Acc. Chem. Res.* **2015**, *48*, 229–237.
- (4) Tsarevsky, N. V.; Matyjaszewski, K. Green” Atom Transfer Radical Polymerization: From Process Design to Preparation of Well-Defined Environmental Friendly Polymeric Materials. *Chem. Rev.* **2007**, *107*, 2270–2299.
- (5) Foster, J. C.; Varlas, S.; Couturaud, B.; Coe, Z.; O’Reilly, R. K. Getting into Shape: Reflections on a New Generation of Cylindrical Nanostructures’ Self-Assembly Using Polymer Building Blocks. *J. Am. Chem. Soc.* **2019**, *141*, 2742–2753.
- (6) Qiu, H.; Russo, G.; Rupar, P. A.; Chabanne, L.; Winnik, M. A.; Manners, I. Tunable Supermicelle Architectures from the Hierarchical Self-Assembly of Amphiphilic Cylindrical B–A–B Triblock Copolymers. *Angew. Chem., Int. Ed.* **2012**, *51*, 11882–11885.
- (7) Pang, X.; He, Y.; Jung, J.; Lin, Z. 1D Nanocrystals with Precisely Controlled Dimensions, Compositions, and Architectures. *Science* **2016**, *353*, 1268–1272.
- (8) Radzinski, S. C.; Foster, J. C.; Scannelli, S. J.; Weaver, J. R.; Arrington, K. J.; Matson, J. B. Tapered Bottlebrush Polymers: Cone-Shaped Nanostructures by Sequential Addition of Macromonomers. *ACS Macro Lett.* **2017**, *6*, 1175–1179.
- (9) Tao, D.; Feng, C.; Lu, Y.; Cui, Y.; Yang, X.; Manners, I.; Winnik, M. A.; Huang, X. Self-Seeding of Block Copolymers with a π -Conjugated Oligo(p-phenylenevinylene) Segment: A Versatile Route toward Monodisperse Fiber-like Nanostructures. *Macromolecules* **2018**, *51*, 2065–2075.
- (10) Barnard, E.; Pfukwa, R.; Maiz, J.; Müller, A. J.; Klumperman, B. Synthesis, Structure, and Crystallization Behavior of Amphiphilic Heteroarm Molecular Brushes with Crystallizable Poly(ethylene oxide) and n-Alkyl Side Chains. *Macromolecules* **2020**, *53*, 1585–1595.
- (11) Kim, K. H.; Kim, M.; Moon, J.; Huh, J.; Bang, J. Bottlebrush Copolymer as Surface Neutralizer for Vertical Alignment of Block Copolymer Nanodomains in Thin Films. *ACS Macro Lett.* **2021**, *10*, 346–353.
- (12) Ren, J. M.; Ishitake, K.; Satoh, K.; Blencowe, A.; Fu, Q.; Wong, E. H. H.; Kamigaito, M.; Qiao, G. G. Stereoregular High-Density Bottlebrush Polymer and Its Organic Nanocrystal Stereocomplex through Triple-Helix Formation. *Macromolecules* **2016**, *49*, 788–795.

- (13) Huang, K.; Jacobs, A.; Rzaev, J. De Novo Synthesis and Cellular Uptake of Organic Nanocapsules with Tunable Surface Chemistry. *Biomacromolecules* **2011**, *12*, 2327–2334.
- (14) Liu, Z.; Huang, Y.; Zhang, X.; Tu, X.; Wang, M.; Ma, L.; Wang, B.; He, J.; Ni, P.; Wei, H. Fabrication of Cyclic Brush Copolymers with Heterogeneous Amphiphilic Polymer Brushes for Controlled Drug Release. *Macromolecules* **2018**, *51*, 7672–7679.
- (15) Huang, K.; Rzaev, J. Charge and size selective molecular transport by amphiphilic organic nanotubes. *J. Am. Chem. Soc.* **2011**, *133*, 16726–16729.
- (16) Lequeieu, J.; Quah, T.; Delaney, K. T.; Fredrickson, G. H. Complete Photonic Band Gaps with Nonfrustrated ABC Bottlebrush Block Polymers. *ACS Macro Lett.* **2020**, *9*, 1074–1080.
- (17) He, Q.; Ku, K. H.; Vijayamohan, H.; Kim, B. J.; Swager, T. M. Switchable Full-Color Reflective Photonic Ellipsoidal Particles. *J. Am. Chem. Soc.* **2020**, *142*, 10424–10430.
- (18) Lu, X.; Tran, T.-H.; Jia, F.; Tan, X.; Davis, S.; Krishnan, S.; Amiji, M. M.; Zhang, K. Providing Oligonucleotides with Steric Selectivity by Brush-Polymer-Assisted Compaction. *J. Am. Chem. Soc.* **2015**, *137*, 12466–12469.
- (19) Tonge, C. M.; Sauve, E. R.; Cheng, S.; Howard, T. A.; Hudson, Z. M. Multiblock Bottlebrush Nanofibers from Organic Electronic Materials. *J. Am. Chem. Soc.* **2018**, *140*, 11599–11603.
- (20) Daniel, W. F. M.; Burdyska, J.; Vatankhah-Varnoosfaderani, M.; Matyjaszewski, K.; Paturej, J.; Rubinstein, M.; Dobrynin, A. V.; Sheiko, S. S. Solvent-Free, Supersoft and Superelastic Bottlebrush Melts and Networks. *Nat. Mater.* **2016**, *15*, 183–189.
- (21) Zhao, S.-Q.; Hu, G.; Xu, X.-H.; Kang, S.-M.; Liu, N.; Wu, Z.-Q. Synthesis of Redox-Responsive Core Cross-Linked Micelles Carrying Optically Active Helical Poly(phenyl isocyanide) Arms and Their Applications in Drug Delivery. *ACS Macro Lett.* **2018**, *7*, 1073–1079.
- (22) Liu, Y.; Wang, Y.; Wang, Y. F.; Lu, J.; Piñon, V.; Weck, M. Shell Cross-Linked Micelle-Based Nanoreactors for the Substrate-Selective Hydrolytic Kinetic Resolution of Epoxides. *J. Am. Chem. Soc.* **2011**, *133*, 14260–14263.
- (23) Venkataraman, S.; Hedrick, J. L.; Ong, Z. Y.; Yang, C.; Ee, P. L.; Hammond, P. T.; Yang, Y. Y. The effects of polymeric nanostructure shape on drug delivery. *Adv. Drug Delivery Rev.* **2011**, *63*, 1228–1246.
- (24) Liu, F.; Zhao, X.; Zhang, X.; Zhang, X.; Peng, J.; Yang, H.; Deng, K.; Ma, L.; Chang, C.; Wei, H. Fabrication of theranostic amphiphilic conjugated bottlebrush copolymers with alternating heterografts for cell imaging and anticancer drug delivery. *Polym. Chem.* **2018**, *9*, 4866–4874.
- (25) Ihara, E.; Takahashi, H.; Akazawa, M.; Itoh, T.; Inoue, K. Polymerization of Various Alkyl Diazoacetates Initiated with (N-Heterocyclic Carbene)Pd/Borate Systems. *Macromolecules* **2011**, *44*, 3287–3292.
- (26) Su, Y.-X.; Xu, L.; Xu, X.-H.; Hou, X.-H.; Liu, N.; Wu, Z.-Q. Controlled Synthesis of Densely Grafted Bottlebrushes That Bear Helical Polyisocyanide Side Chains on Polyisocyanide Backbones and Exhibit Greatly Increased Viscosity. *Macromolecules* **2020**, *53*, 3224–3233.
- (27) Zhulina, E. B.; Sheiko, S. S.; Borisov, O. V. Theory of Microphase Segregation in the Melts of Copolymers with Dendritically Branched, Bottlebrush, or Cycled Blocks. *ACS Macro Lett.* **2019**, *8*, 1075–1079.
- (28) Xiao, L.; Chen, Y.; Zhang, K. Efficient Metal-Free “Grafting Onto” Method for Bottlebrush Polymers by Combining RAFT and Triazolinedione-Diene Click Reaction. *Macromolecules* **2016**, *49*, 4452–4461.
- (29) Kawamoto, K.; Zhong, M.; Gadelrab, K. R.; Cheng, L.-C.; Ross, C. A.; Alexander-Katz, A.; Johnson, J. A. Graft-through Synthesis and Assembly of Janus Bottlebrush Polymers from A-Branch-B Diblock Macromonomers. *J. Am. Chem. Soc.* **2016**, *138*, 11501–11504.
- (30) Liu, W.-B.; Xu, X.-H.; Kang, S.-M.; Song, X.; Zhou, L.; Liu, N.; Wu, Z.-Q. Bottlebrush Polymers Carrying Side Chains on Every Backbone Atom: Controlled Synthesis, Polymerization-Induced Emission, and Circularly Polarized Luminescence. *Macromolecules* **2021**, *54*, 3158–3168.
- (31) Neary, W. J.; Isais, T. A.; Kennemur, J. G. Depolymerization of Bottlebrush Polypentenamers and Their Macromolecular Metamorphosis. *J. Am. Chem. Soc.* **2019**, *141*, 14220–14229.
- (32) Xie, G.; Martinez, M. R.; Olszewski, M.; Sheiko, S. S.; Matyjaszewski, K. Molecular Bottlebrushes as Novel Materials. *Biomacromolecules* **2019**, *20*, 27–54.
- (33) Jellema, E.; Jongerius, A. L.; Reek, J. N. H.; de Bruin, B. C1” Polymerisation and Related C-C Bond forming ‘Carbene Insertion’ Reactions. *Chem. Soc. Rev.* **2010**, *39*, 1706–1723.
- (34) Cahoon, C. R.; Bielawski, C. W. Metal-promoted “C1” polymerizations. *Coord. Chem. Rev.* **2018**, *374*, 261–278.
- (35) Shimomoto, H.; Asano, H.; Itoh, T.; Ihara, E. Pd-Initiated Controlled Polymerization of Diazoacetates with a Bulky Substituent: Synthesis of Well-Defined Homopolymers and Block Copolymers with Narrow Molecular Weight Distribution from Cyclophosphazene Containing Diazoacetates. *Polym. Chem.* **2015**, *6*, 4709–4714.
- (36) Yashima, E.; Ousaka, N.; Taura, D.; Shimomura, K.; Ikai, T.; Maeda, K. Supramolecular Helical Systems: Helical Assemblies of Small Molecules, Foldamers, and Polymers with Chiral Amplification and Their Functions. *Chem. Rev.* **2016**, *116*, 13752–13990.
- (37) Takaya, T.; Oda, T.; Shibasaki, Y.; Hayashi, Y.; Shimomoto, H.; Ihara, E.; Ishibashi, Y.; Asahi, T.; Iwata, K. Excited-State Dynamics of Pyrene Incorporated into Poly(substituted methylene)s: Effects of Dense Packing of Pyrenes on Excimer Formation. *Macromolecules* **2018**, *51*, 5430–5439.
- (38) Tromp, D. S.; Lankelma, M.; de Valk, H.; de Josselin de Jong, E.; de Bruin, B. Aqueous Phase Separation Behavior of Highly Syndiotactic, High Molecular Weight Polymers with Densely Packed Hydroxy-Containing Side Groups. *Macromolecules* **2018**, *51*, 7248–7256.
- (39) Yao, X.-Q.; Wang, Y.-S.; Wang, J. Cp(π -Allyl)Pd-Initiated Polymerization of Diazoacetates: Reaction Development, Kinetic Study, and Chain Transfer with Alcohols. *Macromolecules* **2021**, *54*, 10914–10922.
- (40) Chu, J.-H.; Xu, X.-H.; Kang, S.-M.; Liu, N.; Wu, Z.-Q. Fast Living Polymerization and Helix-Sense-Selective Polymerization of Diazoacetates Using Air-Stable Palladium(II) Catalysts. *J. Am. Chem. Soc.* **2018**, *140*, 17773–17781.
- (41) Li, N.-N.; Li, X.-L.; Xu, L.; Liu, N.; Wu, Z.-Q. Highly Enantioselective and Helix-Sense-Controlled Synthesis of Stereoregular Helical Polycarbenes Using Chiral Palladium(II) Catalysts. *Macromolecules* **2019**, *52*, 7260–7266.
- (42) Wicki, A.; Witzigmann, D.; Balasubramanian, V.; Huwyler, J. Nanomedicine in Cancer Therapy: Challenges, Opportunities, and Clinical Applications. *J. Controlled Release* **2015**, *200*, 138–157.
- (43) Maeda, H.; Nakamura, H.; Fang, J. The EPR Effect for Macromolecular Drug Delivery to Solid Tumors: Improvement of Tumor Uptake, Lowering of Systemic Toxicity, and Distinct Tumor Imaging in Vivo. *Adv. Drug Delivery Rev.* **2013**, *65*, 71–79.